Journal of Pharmaceutical Analysis 13 (2023) 88–98

Contents lists available at ScienceDirect

Journal of Pharmaceutical Analysis

journal homepage: www.elsevier.com/locate/jpa

Original article

Neurotoxicity mechanism of aconitine in HT22 cells studied by microfluidic chip-mass spectrometry

Yingrui Zhang [a, b, 1], Shiyu Chen [a, b, 1], Fangfang Fan [c], Ning Xu [b], Xian-Li Meng [a], Yi Zhang [c, *], Jin-Ming Lin [b, **]

[a] State Key Laboratory of Southwestern Chinese Medicine Resources, School of Pharmacy, Chengdu University of Traditional Chinese Medicine, Chengdu, 611137, China
[b] Beijing Key Laboratory of Microanalytical Methods and Instrumentation, Department of Chemistry, Tsinghua University, Beijing, 100084, China
[c] Ethnic Medicine Academic Heritage Innovation Research Center, Chengdu University of Traditional Chinese Medicine, Chengdu, 611137, China

ARTICLE INFO

Article history:
Received 27 September 2022
Received in revised form
19 November 2022
Accepted 21 November 2022
Available online 23 November 2022

Keywords:
Aconitine
Neurotoxicity mechanism
HT22 cells
Excitatory amino acids
Microfluidic chip-mass spectrometry

ABSTRACT

Aconitine, a common and main toxic component of *Aconitum*, is toxic to the central nervous system. However, the mechanism of aconitine neurotoxicity is not yet clear. In this work, we had the hypothesis that excitatory amino acids can trigger excitotoxicity as a pointcut to explore the mechanism of neurotoxicity induced by aconitine. HT22 cells were simulated by aconitine and the changes of target cell metabolites were real-time online investigated based on a microfluidic chip-mass spectrometry system. Meanwhile, to confirm the metabolic mechanism of aconitine toxicity on HT22 cells, the levels of lactate dehydrogenase, intracellular Ca^{2+}, reactive oxygen species, glutathione and superoxide dismutase, and ratio of Bax/Bcl-2 protein were detected by molecular biotechnology. Integration of the detected results revealed that neurotoxicity induced by aconitine was associated with the process of excitotoxicity caused by glutamic acid and aspartic acid, which was followed by the accumulation of lactic acid and reduction of glucose. The surge of extracellular glutamic acid could further lead to a series of cascade reactions including intracellular Ca^{2+} overload and oxidative stress, and eventually result in cell apoptosis. In general, we illustrated a new mechanism of aconitine neurotoxicity and presented a novel analysis strategy that real-time online monitoring of cell metabolites can provide a new approach to mechanism analysis.

© 2022 The Author(s). Published by Elsevier B.V. on behalf of Xi'an Jiaotong University. This is an open access article under the CC BY-NC-ND license (http://creativecommons.org/licenses/by-nc-nd/4.0/).

1. Introduction

Aconitine is a toxic component of traditional Chinese medicine (TCM), especially *Aconitum* species. It has been reported that *Aconitum* genus exhibits anti-inflammatory, analgesic, immune-regulation, and anti-tumor effects, which plays a beneficial therapeutic role in rheumatism, arthritis, gastroenteritis, various tumors, and certain endocrine disorders [1–4]. However, overuse of TCM containing aconitine in clinic can easily cause poisoning; therefore, it is vital to keep an eye on the limited use of *Aconitum*. Aconitine, belonging to C19-diester diterpene alkaloids, is a kind of highly toxic cardiotoxin and neurotoxin, whose lethal oral dose for human is 1–2 mg [5,6]. Over the last decade, there have been roughly 5,000 cases of aconitine poisoning reported worldwide [7–9]. In such a grim circumstance, figuring out the mechanism of aconitine-induced toxicity is of great benefit to relieving poison effectively and take appropriate treatment. However, research on mechanism of aconitine neurotoxicity is relatively scarce, and thus needs to be explored deeply.

In recent studies, alterations of neurotransmitter content, disorders of ion channels, and induction of cell apoptosis have been verified as the mechanisms of aconitine-induced neurotoxicity [7,10,11]. Nevertheless, the pathway of aconitine leading to neurotoxicity is still to be supplemented. Excitatory amino acids (EAAs), including glutamic acid and aspartic acid, are defined as excitatory neurotransmitters of the central nervous system (CNS). Glutamic acid is the most abundant amino acid present in the CNS and acts as the main excitatory neurotransmitter for the normal functioning of the brain. Stimulation of aconitine can bring about high

Peer review under responsibility of Xi'an Jiaotong University.
* Corresponding author.
** Corresponding author.
E-mail addresses: zhangyi@cdutcm.edu.cn (Y. Zhang), jmlin@mail.tsinghua.edu.cn (J.-M. Lin).
[1] Both authors contributed equally to this work.

https://doi.org/10.1016/j.jpha.2022.11.007
2095-1779/© 2022 The Author(s). Published by Elsevier B.V. on behalf of Xi'an Jiaotong University. This is an open access article under the CC BY-NC-ND license (http://creativecommons.org/licenses/by-nc-nd/4.0/).

extracellular levels of EAAs, especially glutamic acid, excitotoxic to neurons. This can lead to enhanced glycolysis and imbalance of Ca^{2+} homeostasis, which results in excessive Ca^{2+} inflow into neurons. Subsequently, oxidative stress reactions including reactive oxygen species (ROS) formation, glutathione (GSH) reduction, and decrease of superoxide dismutase (SOD) activity occur due to Ca^{2+} overloading, and finally neuronal apoptosis appears [12–14]. There remains the cross-talk among excitatory neurotoxicity, consequent ion transport disorders and oxidative stress, providing a new view for the study on aconitine neurotoxicity mechanism.

Combination of microfluidic chip and mass spectrometry (Chip-MS) technology is of great interest to academic communities focusing on cell analysis and drug research, making parallel screening and biomolecular structures identification linked organically [15]. Recently, our research group has developed a new Chip-MS system to realize real-time online monitoring of the effect of the drugs metabolites on cells, which was utilized for mimicking cellular neurotoxicity in vitro and high-throughput analysis of metabolites to realize exploration of the metabolic process related to neurotoxicity [16–18].

In light of the foundation that HT22 cell line is derived from the hippocampus neuronal precursor cells and lacks functional ionotropic glutamic acid receptors, making it an excellent model to conduct research on glutamic acid-induced oxidative neurotoxicity, we selected HT22 cells as the objects treated with drug in this study [19,20]. Cell metabolites under neurotoxicity reaction were identified and monitored in real time by the Chip-MS system; meanwhile, molecular biotechnology was adopted to investigate the expression of the indexes associated with neurotoxicity after drug stimulation. Finally, the mechanism of aconitine neurotoxicity was concluded by integrating the target metabolites acquired and results of molecular biology test, which revealed that neurotoxicity caused by aconitine occurred for the excitatory neurotoxicity induced by EAAs (Fig. 1). All in all, we illustrated a new mechanism of aconitine neurotoxicity in HT22 cells, which not only laid the foundation for the detoxification of aconitine in clinical research but also provided a superior strategy of mechanism exploration into drug effect.

2. Experimental

2.1. Reagents and materials

HT22 cell lines were purchased from Cell Resource Center, Institute of Basic Medicine (Chinese Academy of Medical Sciences, Beijing, China). Dulbecco's modified Eagle medium (DMEM) (RNBJ7482), 0.25% trypsin with ethylene diamine tetraacetic acid (25200056), and 1% penicillin-streptomycin (15140-122) were obtained from Gibco (Grand Island, NY, USA). Phosphate buffer saline (PBS, 21-040-CVR) and fetal bovine serum (FBS, 35-081-CV) were bought from Corning (Corning, NY, USA). Aconitine (purity > 98%, RP210928), benzoylaconine (purity > 98%, RP210323), and aconine (purity > 99%, RP211011) were purchased from Chengdu Refmedic Technology Co., Ltd. (Chengdu, China). Glutamic acid (purity ≥ 98%, SG8540), aspartic acid (purity ≥ 98%, SA8560), lactic acid (purity ≥ 98%, SL8750), glucose (purity ≥ 98%, SG8150), and dimethylsulfoxide (DMSO) were purchased from Beijing Solarbio Science & Technology Co., Ltd. (Beijing, China). Live/Dead assay kit and Hoechst 33342 were obtained from Gibco. Bcl-2 and Bax enzyme-linked immuno sorbent assay (ELISA) kits were purchased from Jianglai Biotechnology (Shanghai, China). Cell counting kit-8 (CCK-8), 2-(2,7-dichloro-3,6-diacetyloxy-9H-xanthen-9-yl)-benzoic acid (DCFH-DA) solution, fluo-3 acetoxymethyl ester (AM) solution, total SOD assay kit with water-soluble tetrazolium-8 (WST-8), and bicinchoninic acid (BCA) protein concentration assay kit were from Beyotime Biotechnology Company (Beijing, China). Lactate dehydrogenase (LDH) assay kit, reduced GSH assay kit, and Ca^{2+}-ATPase assay kit were purchased from Nanjing Jiancheng Bioengineering

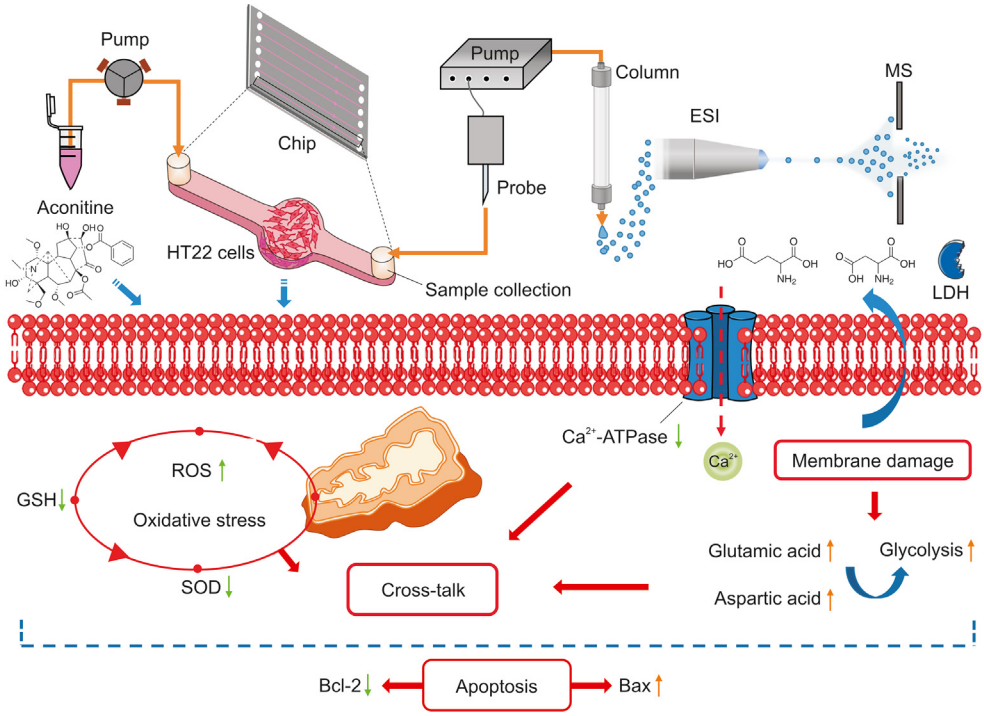

Fig. 1. Schematic illustration of a new mechanism on neurotoxicity induced by aconitine. ESI: electrospray ionization; MS: mass spectrometry; LDH: lactate dehydrogenase; GSH: glutathione; ROS: reactive oxygen species; SOD: superoxide dismutase.

Institute (Nanjing, China). All reagents were of analytical reagent grade and used without further purification. Flow cytometer (BD LSRFortessa SORP, Franklin Lakes, NJ, USA) was used for testing cell apoptosis. Inverted fluorescence microscope (Nikon Stemi 508, Zeiss, Oberkochen, Baden-Württemberg, German) and microplate reader (Varioskan Flash, Thermo Fisher Scientific Inc., Waltham, MA, USA) were used for cell imaging and absorbance measurement. A cell microchip mass spectrometer (Cellent CM-MS 8050, Shimadzu, Kyoto, Japan) was applied to analyze chemical components with a C_{18} column (75 mm × 2.1 mm, 1.7 μm; Shimadzu, Kyoto, Japan).

2.2. Cell culture and treatment

HT22 cells were grown in DMEM supplemented with 10% FBS and 1% penicillin-streptomycin, and incubated under 5% CO_2 at 37 °C. The medium was changed every 2 days, and then the cells were collected to seed in new bottles. Aconitine was dissolved in DMSO as the stock solution (50 mmol/L), which was prepared to series concentrations with the medium in subsequent experiments. The percentage of DMSO in all aconitine treated groups was 0.1%.

2.3. Cytotoxicity assay

The HT22 cells in the logarithmic growth phase (1×10^5 cells) were seeded in a 96-well plate for 12 h and then cultured with different concentrations of aconitine (0, 100, 200, 400, 600, 800, 1000, 1200, 1400, 1600, and 2000 μmol/L) for 24 h. After that, each well was introduced with 10 μL of CCK-8 assay contained in 100 μL of medium at 37 °C for 2 h. Subsequently, the optical density (OD) of each well was measured at 450 nm using a microplate reader.

2.4. Target metabolites screening

The HT22 cells were incubated in static culture for 12 h and divided into three groups including control and two treatment groups. After drug processing for 24 h, the cell supernatant was dealt with acetonitrile addition, vortexed, and then centrifugated for 10 min at 10,000 rpm. Based on the liquid chromatography-triple quadrupole tandem mass spectrometry (LC-QqQ-MS/MS) detection conditions of 96 metabolites established by Shimadzu Corporation [16], changes in the content of cell metabolites associated with excitatory neurotoxicity under different treatments were monitored. The gradient elution conditions and multi-reaction monitoring (MRM) mode of 96 metabolites are shown in Tables S1 and S2, respectively. The peak area statistics of the identified metabolites are shown in Table S3. Meanwhile, the metabolites of aconitine were investigated with comparation of standard substance.

2.5. Chromatographic and mass spectrometric conditions

In this experiment, a Cellent CM-MS system (Shimadzu) was used for cell culture on the chip and metabolite analysis by LC-MS. LC separation was performed by using a C_{18} column equipped with an in-line filter containing replacement frits. The column temperature was maintained at 40 °C. The mobile phase of cell metabolites analysis consisted of 0.1% *(V/V)* aqueous formic acid (solvent A) and 0.1% *(V/V)* formic acid in acetonitrile (solvent B) at a flow rate of 0.3 mL/min, and the gradient elution was completed as follows: 5% B (0–1.0 min), 5%–25% B (1.0–1.5 min), 25%–35% B (1.5–2.0 min), 35%–95% B (2.0–3.0 min), 95%–95% B (3.0–4.0 min), and 95%–5% B (4.0–4.1 min). The mobile phase of aconitine metabolites analysis consisted of 0.2% *(V/V)* aqueous formic acid (solvent A) and methanol (solvent B) at a flow rate of 0.3 mL/min, and the gradient elution was completed as follows: 5% B (0–0.1 min), 5%–40% B (0.1–1.0 min), 40%–65% B (1.0–5.0 min), 65%–65% B (5.0–5.5 min), 65%–90% B (5.5–6.0 min), 90%–90% B (6.0–6.5 min), 90%–40% B (6.5–6.6 min), and 40%–5% B (6.6–6.7 min). The sample was stored in an automatic sampler at 4 °C with an injection volume of 1 μL. The mass spectrometric parameters were conditioned as follows: interface temperature: 300 °C, heating block temperature: 250 °C, desolvation line temperature: 150 °C, spray voltage: 3.00 kV, nebulizer gas (N_2) flow rate: 3 L/min, and heating gas (N_2) and drying gas (N_2) flow rate: 10 L/min. Each component was analyzed using MRM. The positive or negative ion mode of electrospray ionization source was adopted. The MS/MS transitions of each compound analyzed are shown in Table S4.

2.6. Standard substance prepared and standard curves established

The standard substance stock solution of cell metabolites (5 mmol/L) was prepared and diluted with DMEM containing 10% FBS and 1% penicillin-streptomycin to acquire different concentrations and fit a standard curve. Series of concentrations were yielded, ranging from 0.1 to 50 μmol/L in glutamic acid and from 250 to 5000 μmol/L in lactic acid.

2.7. Cell culture on a chip

Polydimethylsiloxane was cast on a silicon wafer by using the standard soft lithography technology, and then bonded to the glass after being dried. The length and width of the microfluidic chip was 6 cm and the thickness was 1 cm. The height of all channels on the microchip was 150 μm. The microchip was brought into operation after sterilized with ultraviolet exposure for 0.5 h and washed three times with PBS. The HT22 cells (1×10^5 cells) were injected into the six microchannels of a microchip, followed with incubation for 12 h under 5% CO_2 at 37 °C. All the microchannels were divided into three groups including the control group and two treatment groups. Then cells were stimulated by corresponding culture medium containing drugs at a rate of 20 μL/h for 24 h through six precise syringe pump units. The photographs of the microchip are shown in Figs. S1A and B. Then, the chip with cells loaded was placed on the Cellent CM-MS device.

2.8. Real-time online quantification of metabolites based on Chip-MS

The Cellent CM-MS device consists of an injection pump unit, cell culture section, LC, changeover valve, and triple quadrupole MS. The injection pump unit continuously pumped out the medium at a flow rate of 20 μL/h while the chip loaded with cells was placed in the device. As is shown in Fig. S1B, after the microchip was set rightly and drugs were channelled tardily, cell metabolites outflowed the other end of the channels and accumulated in collection pools during the flowing culture. The excess liquid was discharged from the outlet of waste after 1 h. The metabolites accumulated within 1 h were detected by the LC-QqQ-MS/MS under MRM mode condition for analysis, in which way the real-time dynamic detection in each hour was realized. The photographs of the Chip-MS device are shown in Fig. S1C.

2.9. LDH release assay

The HT22 cells were plated in 6-well plates (1×10^5 cells) and cultured for 12 h. Subsequently, LDH release was detected in cell supernatant according to the manufacturer's protocol after cells were stimulated with aconitine in different concentrations for 24 h.

The OD levels were measured at 450 nm with a microplate reader.

2.10. Determination of intracellular Ca^{2+} level and Ca^{2+}-ATPase activity

The HT22 cells were plated in confocal wells (1×10^5 cells) and incubated at 37 °C for 12 h. After that, the cells were treated with different dosages of aconitine for 24 h. The Ca^{2+}-specific fluorescent probe Fluo-3 AM diluted to 2 μmol/L was then loaded for 40 min at 37 °C in the dark. After PBS washing and another 20 min incubation, the cells were incubated with Hoechst 33342 for 15 min to stain the nucleus. The inverted fluorescence microscope was used to observe the green fluorescence and the images were analyzed using U.S. National Institute of Health (NIH) ImageJ software. Then cells were cultured in 12-well plates (1×10^5 cells). Cell suspensions were collected with normal saline and ultrasonically broken. Changes in activity of Ca^{2+}-ATPase were detected referring to the kit instructions. The microplate reader was applied to measure the OD values at 636 nm ultimately.

2.11. Measurement of ROS level and GSH and SOD activity

The process of cell seeding and treatment in ROS level measurement was the same as that of intracellular Ca^{2+} detection. The treated cells were then incubated with DCFH-DA diluted to a 1000-fold for 20 min at 37 °C to determine the presence of ROS. Finally, green fluorescence was analyzed applying the inverted fluorescence microscope after the nucleus was stained by Hoechst 33342. Subsequently, the HT22 cells were plated in 12-well plates (1×10^5 cells), cultured for 12 h, and dosed for 24 h. Prior to the formal detection, the protein concentration of each well was calculated by BCA method. The activity of GSH and SOD in lysed cells was both measured with the commercially-available kits, and the absorbances were measured utilizing a microplate reader at 405 and 450 nm, respectively. Both indexes were expressed as U/mg pro.

2.12. Detection of cell apoptosis and protein related to apoptosis

Calcein AM/propidium iodide (PI) double staining kit was used to perform cell apoptosis detection. The HT22 cells were cultured in confocal wells (1×10^5 cells) for 12 h, followed by aconitine administration. The fluorescence probe incubated cells afterwards at 37 °C for 30 min in the dark, and the fluorescence intensity was then observed with a Nikon fluorescent microscope after cells were washed by PBS. The images were analyzed by NIH ImageJ software. Also, cells of different treatment groups seeded in 12-well plates (1×10^5 cells) were gathered and washed with PBS. Then they were loaded with the probe at 37 °C for 30 min and analyzed using flow cytometry. Later, the expressions of pro-apoptotic Bax and anti-apoptotic Bcl-2 proteins were quantitatively measured through ELISA method. After incubation and aconitine stimulation, HT22 cells seeded in 6-well plates were collected in PBS and ultrasonically disrupted. The supernatants were transferred into clean tubes and loaded as samples after centrifugated for 10 min at 10,000 rpm according to the kit's instructions. Eventually, on the basis of the standard curve and the OD values read from a microplate reader, the amount of protein concentration was acquired.

2.13. Data and statistical analysis

Quantitative data were repeated at least three times and presented as the mean ± standard deviation. One-way ANOVA test and Tukey's multiple comparison test were analyzed in GraphPad Prism 8.0.2. In all statistical analyses, the level of significance was set at $P < 0.05$.

3. Results

3.1. Aconitine induced cytotoxicity in HT22 cells

The cytotoxicity of aconitine on HT22 cells was detected via CCK-8 assay. As is shown in Figs. S2A and B, cells treated with aconitine exhibited lower cell viability, which significantly decreased after stimulation of aconitine over 200 μmol/L for 24 h compared with control group and appeared to be concentration-dependent. The 50% inhibitory concentration was revealed to be 908.1 μmol/L in Fig. S2C, and while the viability of cells was about 80% and 60%, aconitine concentration was 400 and 800 μmol/L, respectively. On this basis, we chose these two concentrations for subsequent experiments.

3.2. Dynamic change of target differential metabolites screened in different treated groups

To explore the differences in target metabolites, especially EAAs among diverse treatment groups of HT22 cells, the cell supernatants were collected with stimulation of 0, 400, and 800 μmol/L aconitine for 24 h and investigated by LC-QqQ-MS/MS after vortexing and centrifugation. According to the *m/z* value and the fragmentation patterns of 96 metabolites, there were 40 metabolites identified in the end, including metabolites correlated to excitatory neurotoxicity such as glutamic acid and aspartic acid. Subsequently, the peak area of each metabolite was relatively quantified, and the peak area ratios of each group versus control group were calculated. The differential change of 40 metabolites in different groups is shown in Fig. 2A and principal component analysis (PCA) is shown in Fig. S3. It can be seen that the expression of metabolites in each group had great differences and good discrimination. The result of heatmap demonstrated that glutamic acid and aspartic acid increased subsequently with the increase of aconitine concentration. Literature has shown that glutamic acid can promote glycolysis, resulting in the reduction of glucose and the accumulation of lactic acid level [21], which is consistent with the consequence of the heatmap. In this foundation, glutamic acid, aspartic acid, lactic acid, and glucose were screened as target metabolites for further analysis, which all had significant differences after drug stimulation in comparison with unprocessed group (Figs. 2B–E).

By making use of standard substances, the fragment ions and fragmentation patterns of the four target metabolites were analyzed according to product ion scan mode and the consequences are shown in Figs. 2F–I. The chromatograms of four target metabolites under MRM mode are shown in Fig. S4. Glutamic acid showed precursor-to-product transitions at *m/z* 148.10 → 84.10 (Fig. 2F), aspartic acid exhibited precursor-to-product transitions at *m/z* 134.10 → 74.15 (Fig. 2G), the precursor-to-product transitions of lactic acid occurred at *m/z* 89.15 → 43.10/45.30 (Fig. 2H), and glucose performed precursor-to-product transitions at *m/z* 179.15 → 89.05 (Fig. 2I).

In view of the literature reports, we speculated that the aconitine metabolites may include benzoylaconine and aconine. To verify the inference, the standard substances of aconitine, benzoylaconine, and aconine as well as the samples obtained from groups treated by aconitine were detected according to the characteristic fragment peaks applying MS/MS spectra under the MRM mode. As is shown in Fig. S5, the retention time of three tested compounds in the sample was equal to that of reference substances for each one, which indicated that benzoylaconine and aconine, two newly synthesized components after HT22 cells stimulated by aconitine, were metabolized by aconitine. The structures of characteristic fragments and metabolic processes of aconitine in HT22 cells are shown in Fig. 3.

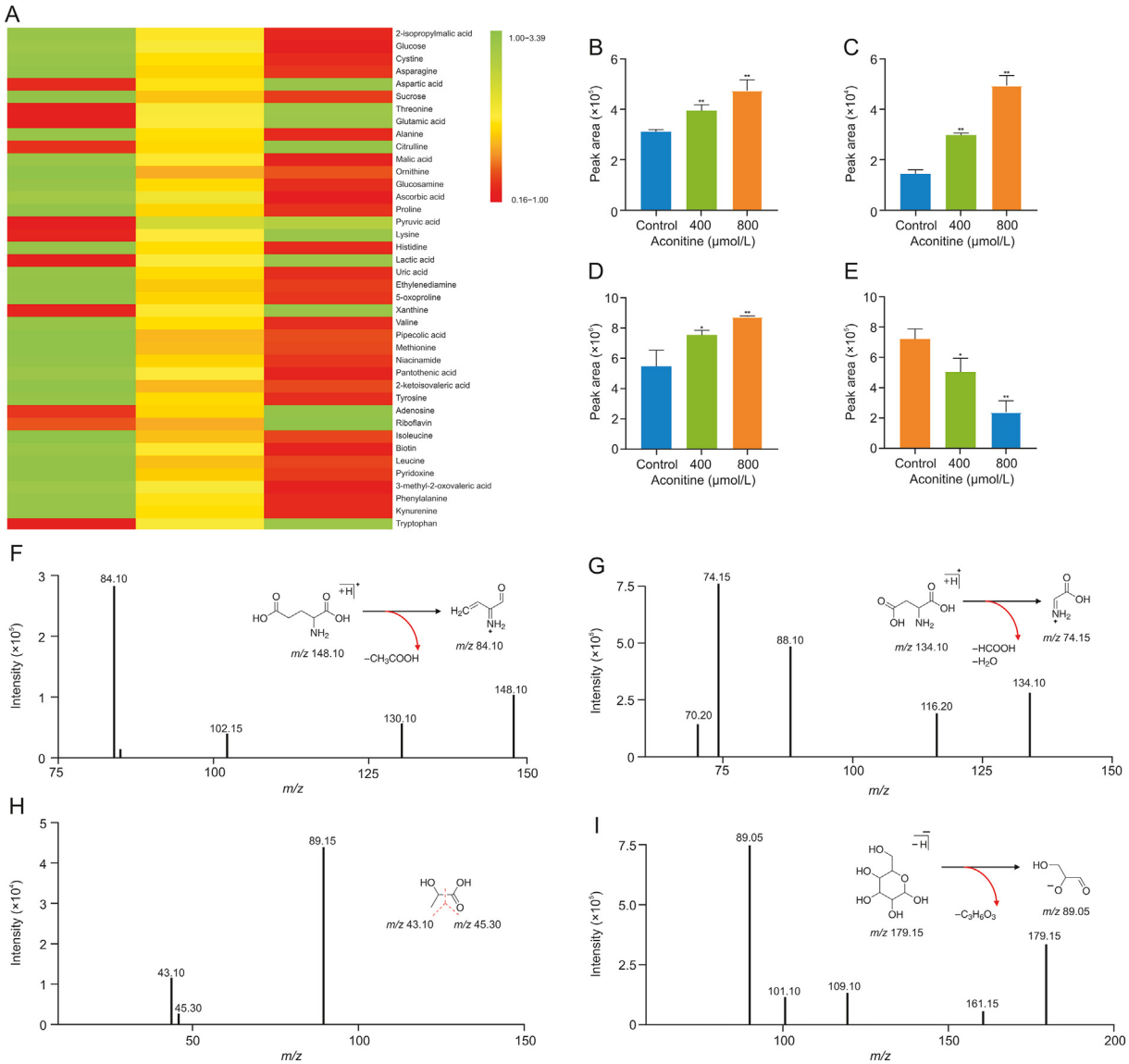

Fig. 2. Differential metabolites in HT22 cells and fragment ion analysis of four target metabolites. Data are shown as mean ± standard deviation ($n = 3$) for each protocol of experiment. (A) Heatmap of 40 metabolites under different groups. The difference analysis of peak area of (B) glutamic acid, (C) aspartic acid, (D) lactic acid, and (E) glucose under stimulation of aconitine at different concentrations. Characteristic fragment structure of (F) glutamic acid, m/z 148.10 → 84.10; (G) aspartic acid, m/z 134.10 → 74.15; (H) lactic acid, m/z 89.15 → 43.10/45.30; and (I) glucose, m/z 179.15 → 89.05. * $P < 0.05$ and ** $P < 0.01$, comparison between groups of different aconitine concentrations and control group.

Herein, glutamic acid and lactic acid had more release, which made quantitative analysis easier and more accurate. Therefore, these two cell metabolites were monitored to reveal the dynamic change of content afterwards. The standard curves of metabolites having good linear relations were established as is shown in Fig. S6. The limit of quantitation of glutamic acid and lactic acid was 0.04 and 24.75 μmol/L, respectively, based on signal-to-noise ratio = 10.

Based on the standard curve, the content of glutamic acid and lactic acid in extracellular fluid was monitored in real time every hour during dynamic culture for 24 h, and the changes of glutamic acid and lactic acid in each group at different time were plotted as line charts, which is shown in Fig. 4. Obviously, the change of glutamic acid (Fig. 4A) and lactic acid (Fig. 4B) showed differences in different groups with the increasing time, and data of each group were collected for statistical analysis. The results indicated that when cells were treated with aconitine, the levels of glutamic acid (Fig. 4C) and lactic acid (Fig. 4D) significantly increased compared to the control group, which was consistent with the results of heatmap.

3.3. Aconitine led to LDH extravasation

LDH is a common glycolytic enzyme in cells. The level of LDH release is a key indicator of cell membrane integrity, which means LDH in extracellular medium increases significantly when the cell membrane structure is damaged [22]. Therefore, evaluation of LDH leakage was considered as a criterion to test cell membrane integrity in this study. As is shown in Fig. 5A, a significant increase in LDH extravasation was observed after the exposure of cells to aconitine compared with the control group, and the release showed direct proportion to aconitine concentration. As a result, it was concluded that stimulation of aconitine could induce the increase of LDH release, which confirmed that aconitine caused significant damage to membrane integrity in a dose-dependent manner.

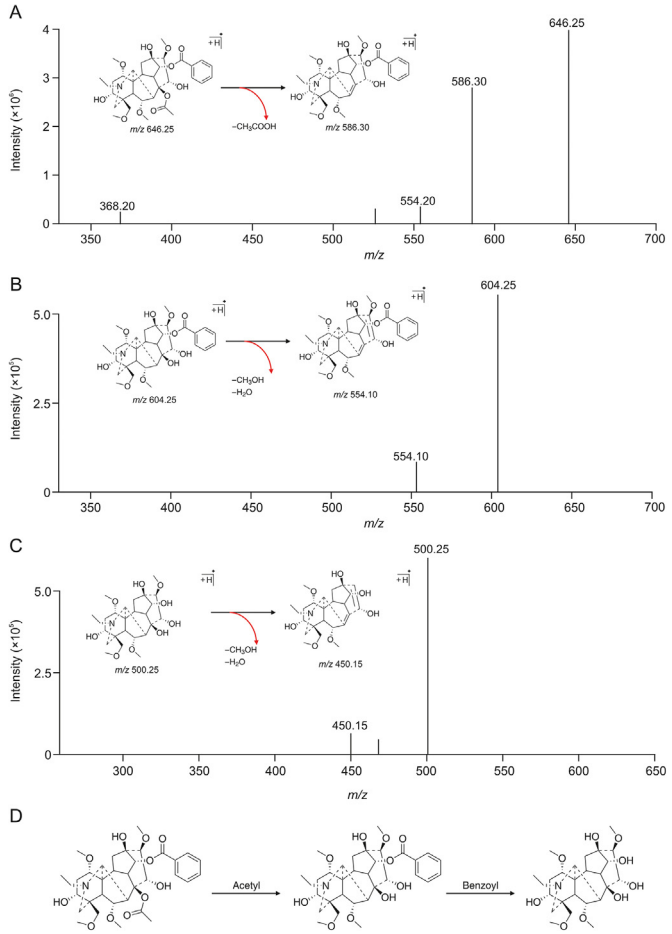

Fig. 3. The metabolic process of aconitine in HT22 cells. (A) Aconitine, *m/z* 646.25 → 586.30; (B) Benzoylaconine, *m/z* 604.25 → 554.10; (C) Aconine, *m/z* 500.25 → 450.15; (D) The two metabolite processes of aconitine in HT22 cells.

3.4. Aconitine resulted in intracellular Ca^{2+} overload and oxidative damage

A rapid Ca^{2+} influx can be induced by excessive glutamic acid, leading to sustained rise in intracellular Ca^{2+} [23]. We then investigated the effect of aconitine on the concentration of intracellular Ca^{2+} using Fluo-3 AM probe. As is shown in Figs. 5B and C, a dramatic increase in the intracellular Ca^{2+} level was detected after exposure of 400 and 800 μmol/L aconitine for 24 h in HT22 cells, triggering about 1.36 and 2.55 folds of increase in fluo-3 fluorescence intensity comparing to the control group, respectively. In contrast, the activities of the Ca^{2+}-ATPase decreased significantly after aconitine treatment [24] (Fig. 5D). It was well indicated that aconitine-induced increase of glutamic acid could cause intracellular Ca^{2+} overload, disrupting the homeostasis of Ca^{2+}.

Glutamic acid at higher concentrations as well as Ca^{2+} overloading has been shown to induce oxidative stress in neurons [25,26]. Noteworthily, the accumulation of ROS might occur due to GSH depletion, which could also lead to the consumption of SOD [27]; hence, the above indicators were considered to evaluate levels of oxidative stress damage. As is shown in Fig. 6A, in comparison with the control group, GSH levels of groups treated with 400 and 800 μmol/L aconitine were decreased significantly and descended to 56% and 50%, respectively. To observe aconitine-induced alterations of intracellular ROS levels, DCFH-DA was used as a probe to stain (Figs. 6B and C). It could be obtained according to fluorescence levels that aconitine treatment increased ROS levels in HT22 cells significantly. We also measured the enzyme activities of SOD as is shown in Fig. 6D, which diminished to 72% and 57% of control levels in the 400 and 800 μmol/L aconitine groups, respectively. These consequences suggested that aconitine treatment increased the generation of ROS and oxidative stress levels, which played an important role in glutamic acid-induced excitatory toxicity and apoptosis.

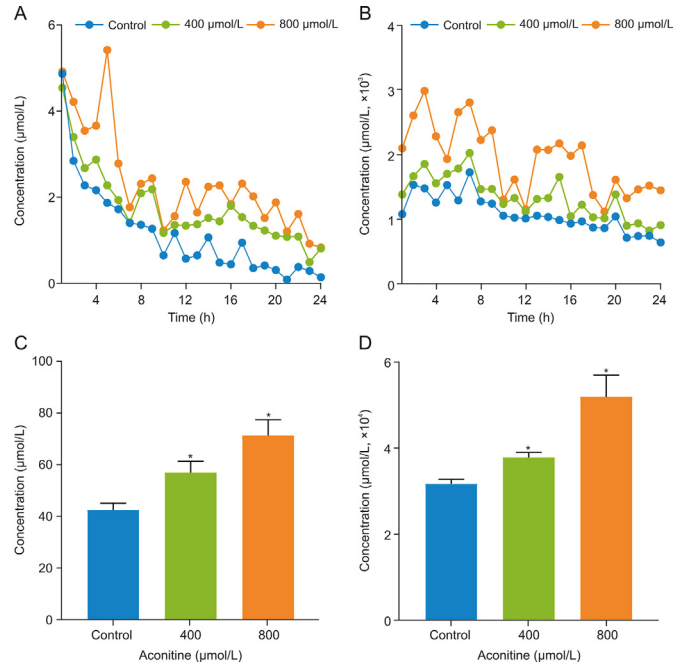

Fig. 4. Real-time detection and quantification analysis of cell metabolites. Data are shown as mean ± standard deviation ($n = 3$) for each protocol of experiment. Changes of (A) glutamic acid and (B) lactic acid under different treated groups from 1 h to 24 h. Statistical analysis of total concentration of (C) glutamic acid and (D) lactic acid under treatment of different aconitine concentrations. $^{*}P < 0.01$, comparison between groups of different aconitine concentrations and control group.

3.5. Aconitine could promote cell apoptosis

Previously, it has been shown that glutamic acid-induced oxidative stress led to neuronal apoptosis via modulating the expression of Bcl-2 family proteins in a form of increasing the ratio of Bax to Bcl-2. To observe the levels of cell apoptosis induced by aconitine, calcein-AM and PI was used as two kinds of probes to perform double fluorescence staining, which made the living cells present green fluorescence while the dead cells showed red fluorescence. As is shown in Figs. 7A–D, the groups treated with aconitine both exhibited significant increase in red fluorescence intensity and apoptosis rate which was assayed by flow cytometry.

The expressions of Bax and Bcl-2 proteins and Bax/Bcl-2 ratio were assessed by ELISA kit (Figs. 7E and F). Compared with the control group, 24 h after aconitine treatment, Bax protein expression increased, while Bcl-2 protein expression decreased. However, there was no significant difference in protein concentration changes of neither Bax nor Bcl-2. Remarkably, the ratio of Bax/Bcl-2 ascended with the rising concentration of aconitine and both groups stimulated by aconitine showed significant differences compared to the control group, which indicated that interventional procedures of aconitine could modify the Bax/Bcl-2 proteins ratio and ultimately induce cell apoptosis.

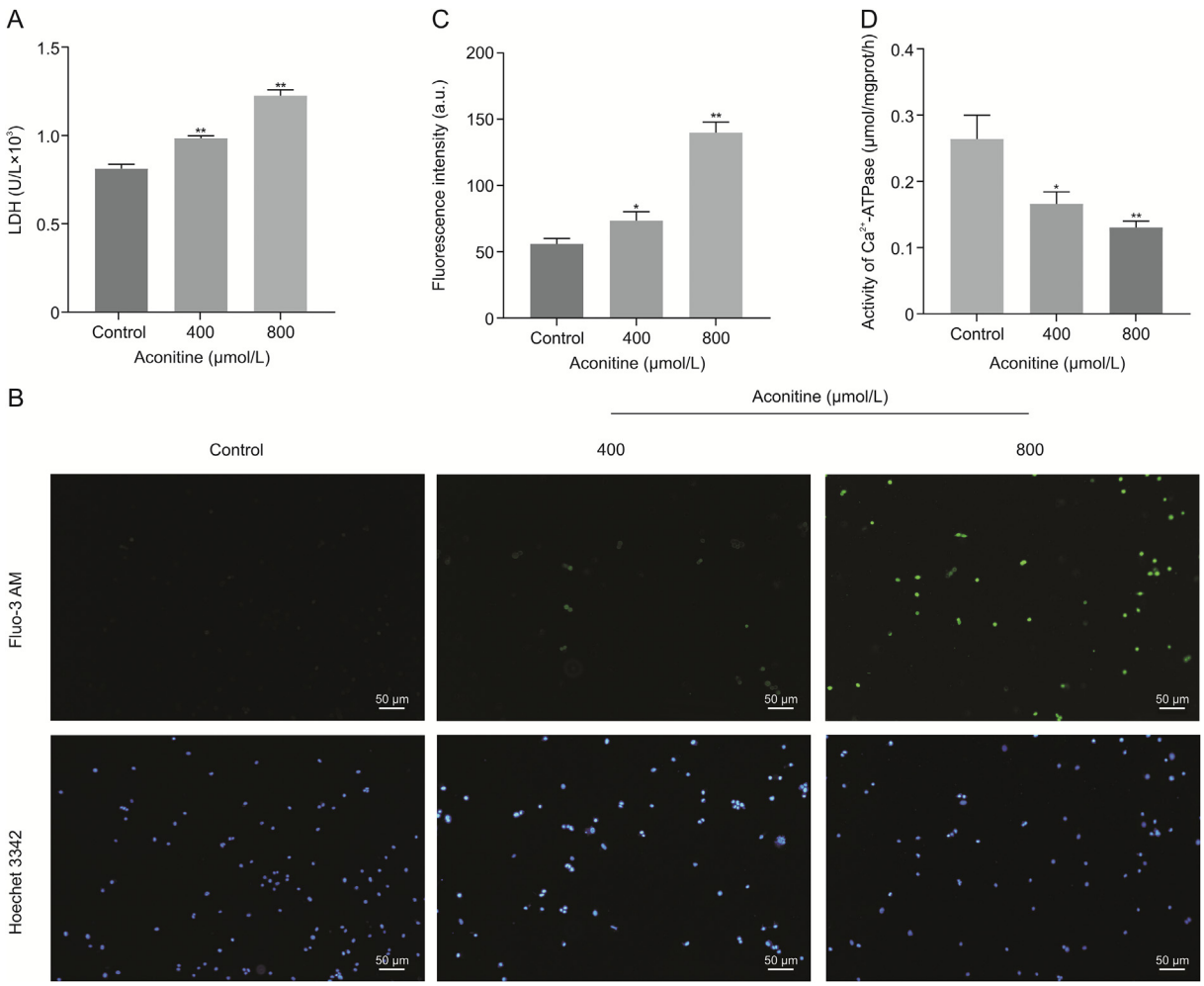

Fig. 5. Changes of extracellular lactate dehydrogenase (LDH) and intracellular Ca^{2+} after aconitine treatment. Data are shown as mean ± standard deviation ($n = 3$) for each protocol of experiment. (A) LDH levels of different concentrations of aconitine treated in HT22 cells. (B) Fluorescent imaging and (C) fluorescence intensities of intracellular Ca^{2+} levels after aconitine treatment. (D) Effect of aconitine stimulation on activity of Ca^{2+}-ATPase. * $P < 0.05$ and ** $P < 0.01$, comparison between groups of different aconitine concentrations and control group. AM: acetoxymethyl ester.

4. Discussion

Herbal medicines are commonly used all over the world for thousands of years. With the increasing popularity of herbal drugs, herb-induced fatal poisoning cases, taking *Aconitum* as an example, have frequently occurred as a result of inappropriate usage, overdose, long-term consumption, or poor quality [28]. Plants belonging to *Aconitum* genus of *Ranunculaceae* family have been extensively applied to treat multiple diseases, in which aconitine is one of the major bioactive and toxic alkaloids frequently employed for its anti-inflammatory, analgesic, anti-rheumatic, and cardiotonic actions [29]. However, aconitine has severe cardiotoxicity and neurotoxicity, making it hard to identify its safe dosage range. Thus, it is of great concern to researchers exploring the toxic mechanism and attenuated methods of aconitine. The typical clinical features of aconitine neurotoxicity involve CNS diseases such as involuntary tremors and paroxysmal convulsion [30,31]. However, the neurotoxic mechanisms of aconitine remain poorly understood. Therefore, it is expected that the mechanism of central neurotoxicity induced by aconitine deserves in-depth exploration so as to determine the poison range of aconitine, provide a method for detoxification, and finally ensure its safety in clinical use [32].

In this study, we found that aconitine could significantly increase the content of EAAs such as glutamic acid and aspartic acid in the supernatant of HT22 cells belonging to neurons in the CNS. EAAs participated in synaptic excitatory transmission and promoted learning and memory in physiological status. However, prolonged exposure to excessive EAAs can overly activate their receptors and evoke significant effects on neural cells through the generation of neurotoxic or excitotoxic cascades [33,34] and increase sensitivity to excitotoxic injury. Therefore, the significant increase of glutamic acid and aspartic acid after stimulation might be one of the pathogenesis of aconitine neurotoxicity. In addition, the significant accumulation of extracellular lactic acid and decrease of glucose suggested enhanced anaerobic glycolysis, which has been documented for the association with neurotoxicity [35]. In view of the buildup of lactic acid accelerating lactic acidosis and oxidative injury [36,37], it might be one of the critical factors in cell damage caused by EAAs. Moreover, the results of dynamic monitoring on glutamic acid and lactic acid also confirmed the above inference.

Lactic acid could be converted from pyruvate with LDH catalyzing [38]. Moreover, the increase of extracellular LDH levels was correlated to the destruction of cell membrane integrity. In our study, the levels of extracellular LDH increased significantly after

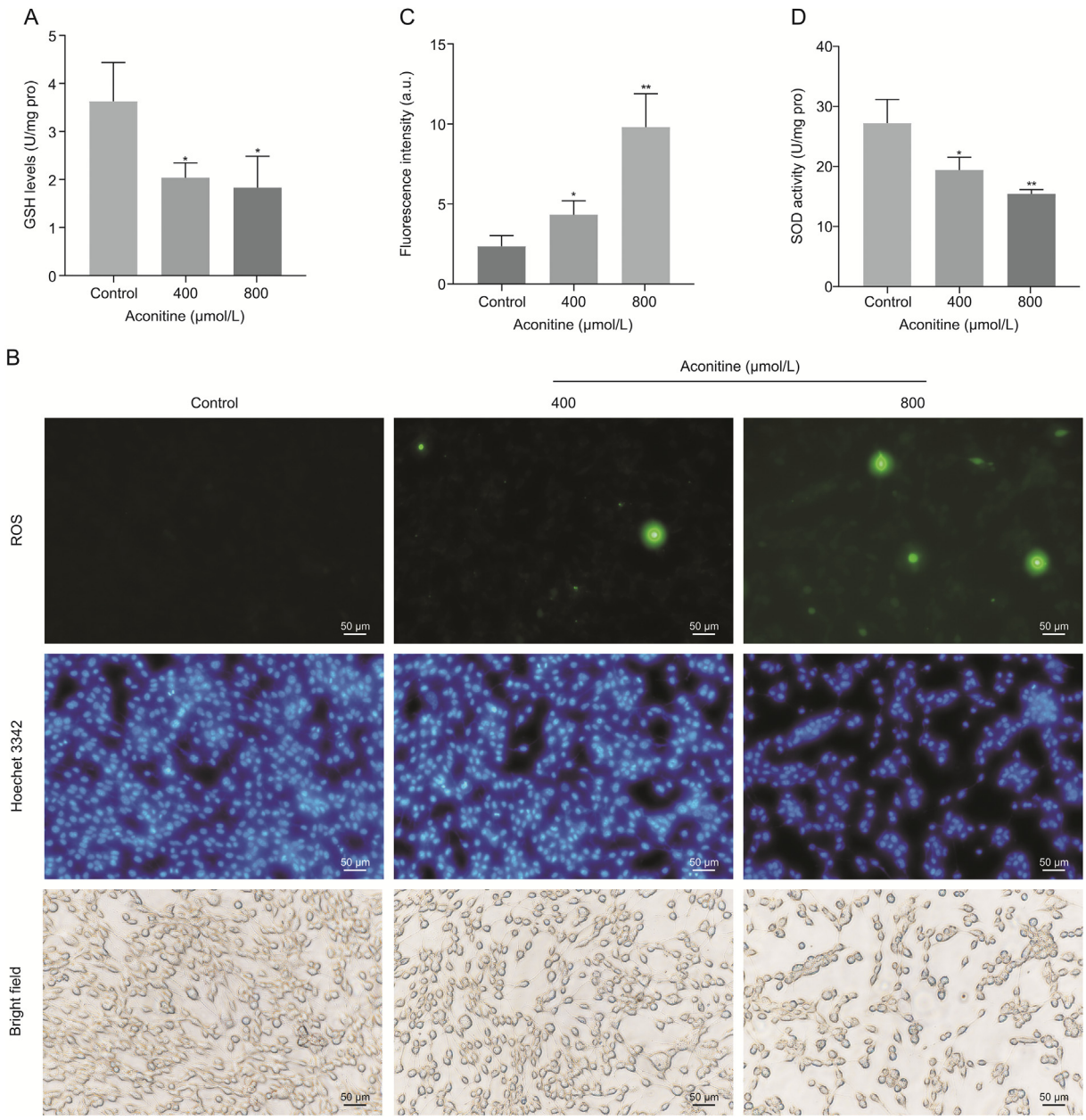

Fig. 6. Oxidative stress response after aconitine stimulation. Data are shown as mean ± standard deviation ($n = 3$) for each protocol of experiment. (A) Influence of aconitine on glutathione (GSH) levels in HT22 cells. (B) Fluorescent imaging and (C) fluorescence intensities of reactive oxygen species (ROS) production in HT22 cells treated by different concentrations of aconitine. (D) The detection of superoxide dismutase (SOD) activity after aconitine stimulation. $^{*}P < 0.05$ and $^{**}P < 0.01$, comparison between groups of different aconitine concentrations and control group.

aconitine treatment, indicating that aconitine could result in cell membrane damage. Furthermore, the overspill of EAAs induced by the disruption of cell membrane was considered to be one of the causes of the elevation of EAAs levels in cell supernatant.

It is notable that a rapid Ca^{2+} influx can be induced by excessive glutamic acid, leading to an increase of intracellular Ca^{2+} concentration and deregulation of Ca^{2+} homeostasis. In neurons, Ca^{2+} overloading results in generation of ROS and oxidative stress [12]. Previous studies have reported that excessive concentrations of extracellular glutamic acid prevented cysteine uptake, followed by blocked synthesis of intracellular GSH and its concentration decreasing. Similarly, efflux of glutamic acid and decreased intracellular glutamic acid could reduce GSH synthesis as well. GSH depletion leads to the accumulation of ROS and the consumption of SOD enzyme [12,27,33,39]. Our experimental results suggested that the intracellular Ca^{2+} level of HT22 cells was significantly increased and the activity of Ca^{2+}-ATPase was significantly inhibited after aconitine stimulation. Also, a significant increase of intracellular ROS level was detected, while GSH level and SOD activity showed significant decrease. It can be seen that aconitine damaged enzymatic and nonenzymatic defense systems, thereby stimulating the generation of oxidative stress.

It is reported that the overproduction of ROS can lead to nonreceptor-mediated toxicity, making oxidative stress considered to be a major cause of neuronal cell death in acute brain injury [23]. Moreover, oxidative stress can cause mitochondria damage, disrupting intracellular Ca^{2+} storage, and exacerbating Ca^{2+}

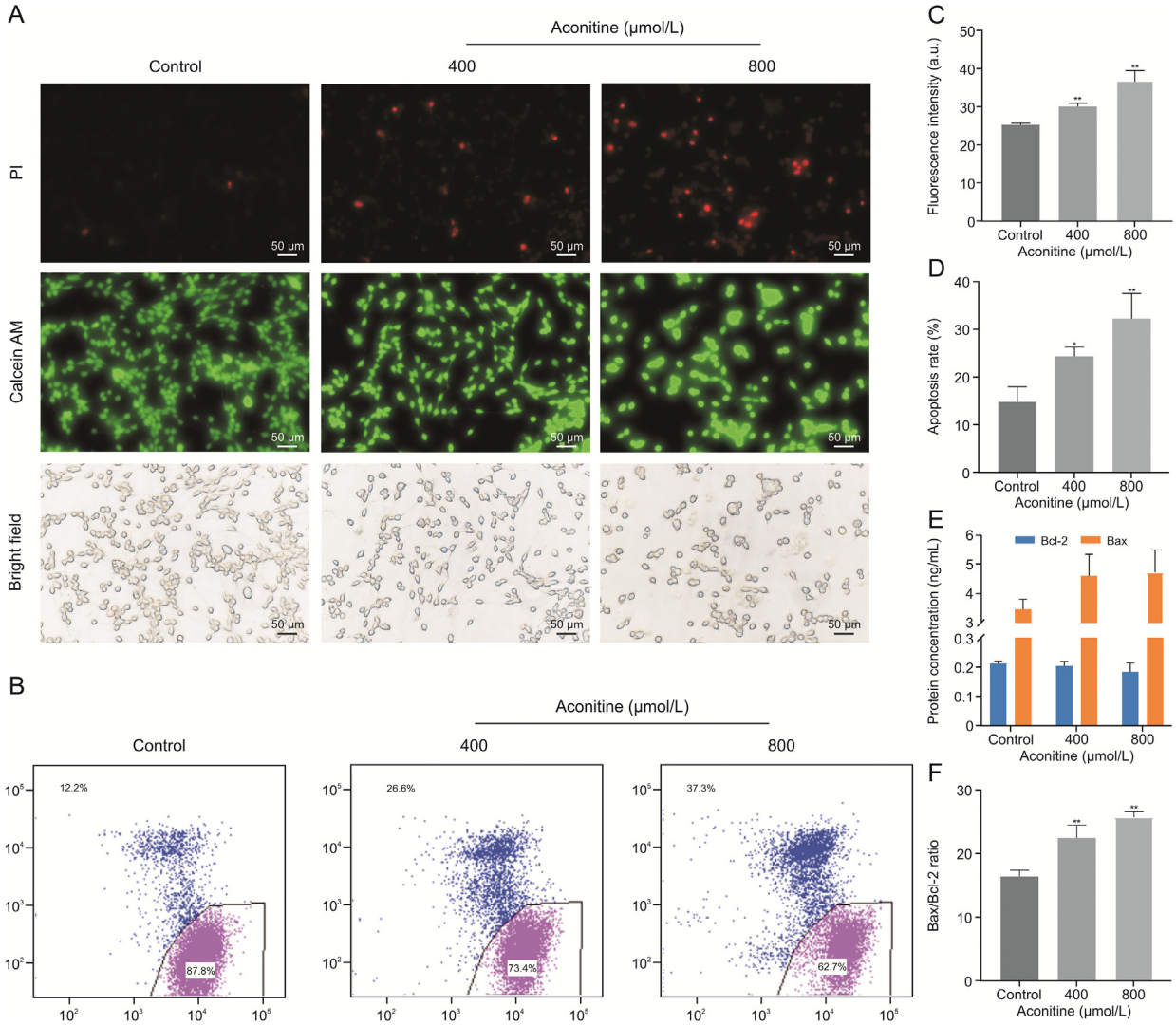

Fig. 7. Effects of aconitine on apoptosis of HT22 cells. Data are shown as mean ± standard deviation ($n = 3$) for each protocol of experiment. (A) Fluorescence imaging of live/dead levels and (B) flow cytometry imaging after HT22 cells treated by different concentrations of aconitine. (C) Fluorescence intensities of dead cells and (D) cell apoptosis rate after exposure of HT22 cells with aconitine. (E) The respective expression of Bax and Bcl-2 in HT22 cells stimulated by aconitine. (F) The changes of Bax and Bcl-2 ratio after aconitine treatment. $^{*}P < 0.05$ and $^{**}P < 0.01$, comparison between groups of different aconitine concentrations and control group. PI: propidium iodide; AM: acetoxymethyl ester.

overloading. Oxidative damage inhibits glutamic acid uptake via direct interactions with glutamic acid transporter proteins, which would further bring about a sustained increase in extracellular glutamic acid and reduction of intracellular GSH generation, creating a vicious circle. Therefore, there exists a cross-talk among the excitatory neurotoxicity of EAAs, intracellular Ca^{2+} overload, and oxidative stress. It has a similarity to the positive feedback regulation under pathological conditions, further aggravating the neurotoxicity caused by aconitine.

Previously, it has been shown that glutamic acid induces neuronal apoptosis via modulating the expression of Bcl-2 family proteins. Additionally, the rapid increase of intracellular Ca^{2+} concentration has been confirmed to have association with the elevation of pro-apoptotic protein Bax and the decrease of anti-apoptotic protein Bcl-2, resulting in the loss of integrity of mitochondrial membrane and eventually apoptosis [23,40]. In this study, aconitine medication increased the ratio of Bax to Bcl-2 and led to neuronal apoptosis, indicating that Bax/Bcl-2 apoptotic pathway is involved in the aconitine neurotoxicity.

Above all, aconitine is neurotoxic and can induce apoptosis of HT22 cells. The excessive concentration of extracellular EAAs induced by aconitine can lead to excitatory toxicity, and then a series of cascade reactions such as Ca^{2+} influx and oxidative stress occur, and eventually apoptosis appears in cells by the regulation of Bax/Bcl-2 pathway.

In the study, Chip-MS device has been successfully applied to explore cell metabolism and mechanism of cytotoxicity, realizing the real-time analysis of cell metabolites during dynamic cell culture and enabling a more realistic and intuitive investigation of the occurrence and development of aconitine-induced neurotoxicity. However, it must be admitted that there are still some limitations. Firstly, the device is expensive and occupies large space, which makes its application inconvenient and hinders the large-scale promotion. Another challenge we face is how to maintain the cell viability in microchips. It is suggested that the Chip-MS device can be developed to be more portable, and the cell culture assembly for well culturing needs optimizing. Furthermore, chips with more advanced functions connected to MS, such as

organ or single cell on chip, can provide a powerful mode for mimicking drug metabolism, cytotoxicity assessment, disease diagnosis, and gene analysis, which deserves more attention in future development [41,42].

5. Conclusion

In conclusion, we revealed a new mechanism and concluded that aconitine could induce neurotoxicity by excitatory toxicity of EAAs in excess. Subsequently, increased glycolysis including lactic acid accumulation and glucose consumption further exacerbated cell damage. In addition, excitatory neurotoxicity could bring about intracellular Ca^{2+} overload and oxidative stress response, which caused damage to mitochondria, and ultimately led to cell apoptosis in Bax/Bcl-2 pathway regulation. In this study, we confirmed a novel analysis strategy integrating Chip-MS system analysis and biomolecular analysis, which was successfully applied to uncover the molecular changes in the aconitine neurotoxicity and metabolites under neurons. The presented method opened a way of real-time dynamic online monitoring of the target molecules and mechanism associated with drugs on cells, and it provided a superior strategy to discover a method for detoxification of aconitine and ensure its safety in clinical use.

CRediT author statement

Yingrui Zhang and **Shiyu Chen:** Investigation, Conceptualization, Methodology, Data curation, Formal analysis, Writing - Original draft preparation; **Fangfang Fan:** Validation; **Ning Xu:** Visualization; **Xian-Li Meng**, **Yi Zhang**, and **Jin-Ming Lin:** Supervision, Project administration, Funding acquisition.

Declaration of competing interest

The authors declare that there are no conflicts of interest.

Acknowledgments

This research was supported the National Natural Science Foundation of China (Grant Nos.: 81973569, 82130113, and 22034005), the National Key R&D Program of China (Grant No.: 2021YFF0600700), and the “Xinglin Scholars” Research Promotion Program of Chengdu University of Traditional Chinese Medicine (Grant No.: BSH2021009).

Appendix A. Supplementary data

Supplementary data to this article can be found online at https://doi.org/10.1016/j.jpha.2022.11.007.

References

[1] F. Peng, N. Zhang, C. Wang, et al., Aconitine induces cardiomyocyte damage by mitigating BNIP3-dependent mitophagy and the TNFα-NLRP3 signalling axis, Cell Prolif 53 (2020), e12701.
[2] X. Li, L. Gu, L. Yang, et al., Aconitine: A potential novel treatment for systemic lupus erythematosus, J. Pharmacol. Sci. 133 (2017) 115–121.
[3] E. Nyirimigabo, Y. Xu, Y. Li, et al., A review on phytochemistry, pharmacology and toxicology studies of *Aconitum*, J. Pharm. Pharmacol. 67 (2014) 1–19.
[4] X. Wang, H. Wang, A. Zhang, et al., Metabolomics study on the toxicity of aconite root and its processed products using ultraperformance liquid-chromatography/electrospray-ionization synapt high-definition mass spectrometry coupled with pattern recognition approach and ingenuity pathways analysis, J. Proteome Res. 11 (2012) 1284–1301.
[5] C. Peng, T. Zheng, F. Yang, et al., Study of neurotoxic effects and underlying mechanisms of aconitine on cerebral cortex neuron cells, Arch Pharm. Res. 32 (2009) 1533–1543.
[6] T. Chan, Aconite poisoning, Clin. Toxicol. (Phila.) 47 (2009) 279–285.
[7] L. Yang, Y. Chen, J. Zhou, et al., Aconitine induces mitochondrial energy metabolism dysfunction through inhibition of AMPK signaling and interference with mitochondrial dynamics in SH-SY5Y cells, Toxicol. Lett. 347 (2021) 36–44.
[8] H. Li, L. Liu, S. Zhu, et al., Case reports of aconite poisoning in mainland China from 2004 to 2015: A retrospective analysis, J. Forensic. Leg. Med. 42 (2016) 68–73.
[9] G. Lu, Z. Dong, Q. Wang, et al., Toxicity assessment of nine types of decoction pieces from the daughter root of *Aconitum carmichaeli* (Fuzi) based on the chemical analysis of their diester diterpenoid alkaloids, Planta Med. 76 (2010) 825–830.
[10] A. Sterea, S. Almasi, Y. Hiani, The hidden potential of lysosomal ion channels: A new era of oncogenes, Cell Calcium 72 (2018) 91–103.
[11] S. Hsu, W. Liang, Cytotoxic effects of mesaconitine, the *Aconitum carmichaelii* debx bioactive compound, on HBEC-5i human brain microvascular endothelial cells: Role of Ca^{2+} signaling-mediated pathway, Neurotox. Res. 39 (2021) 256–265.
[12] Y. Deng, Z. Xu, B. Xu, et al., Exploring cross-talk between oxidative damage and excitotoxicity and the effects of riluzole in the rat cortex after exposure to methylmercury, Neurotox. Res. 26 (2014) 40–51.
[13] L. Zhang, L. Hao, H. Wang, et al., Neuroprotective effect of resveratrol against glutamate-induced excitotoxicity, Adv. Clin. Exp. Med. 24 (2015) 161–165.
[14] S. Maya, T. Prakash, K. Madhu, Assessment of neuroprotective effects of Gallic acid against glutamate-induced neurotoxicity in primary rat cortex neuronal culture, Neurochem. Int. 121 (2018) 50–58.
[15] M. Jie, S. Mao, H. Li, et al., Multi-channel microfluidic chip-mass spectrometry platform for cell analysis, Chin. Chem. Lett. 28 (2017) 1625–1630.
[16] F. Fan, N. Xu, Y. Sun, et al., Uncovering the metabolic mechanism of salidroside alleviating microglial hypoxia inflammation based on microfluidic chip-mass spectrometry, J. Proteome Res. 21 (2022) 921–929.
[17] N. Xu, H. Lin, S. Lin, et al., A fluidic isolation-assisted homogeneous-flow-pressure chip-solid phase extraction-mass spectrometry system for online dynamic monitoring of 25-hydroxyvitamin D_3 biotransformation in cells, Anal. Chem. 93 (2021) 2273–2280.
[18] S. Han, P. Zhang, H. Lin, et al., Real-time monitoring the efficacy of 7-hydroxycoumarin to cells cultured on microfluidics in different extracellular pH environments by chip-mass spectrometry, Talanta 243 (2022), 123331.
[19] Y. Hao, S. Bai, J. Peng, et al., TRIM27-mediated ubiquitination of PPARγ promotes glutamate-induced cell apoptosis and inflammation, Exp. Cell Res. 400 (2021), 112437.
[20] K. Pathakoti, L. Goodla, M. Manubolu, et al., Metabolic alterations and the protective effect of punicalagin against glutamate-induced oxidative toxicity in HT22 cells, Neurotox. Res. 31 (2017) 521–531.
[21] B. Alessandri, H. Landolt, H. Langemann, et al., Application of glutamate in the cortex of rats: A microdialysis study, Acta Neurochir. Suppl. 67 (1996) 6–12.
[22] W. Wang, J. Zhang, Z. Qiu, et al., Effects of polyethylene microplastics on cell membranes: A combined study of experiments and molecular dynamics simulations, J. Hazard Mater. 429 (2022), 128323.
[23] X. Lin, Y. Zhao, S. Li, Astaxanthin attenuates glutamate-induced apoptosis via inhibition of calcium influx and endoplasmic reticulum stress, Eur. J. Pharmacol. 806 (2017) 43–51.
[24] D. Roos, R. Seeger, R. Puntel, et al., Role of calcium and mitochondria in mehg-mediated cytotoxicity, J. Biomed. Biotechnol. 2012 (2012), 248764.
[25] J.H. Song, M.-S. Shin, G.S. Hwang, et al., Chebulinic acid attenuates glutamate-induced HT22 cell death by inhibiting oxidative stress, calcium influx and MAPKs phosphorylation, Bioorg. Med. Chem. Lett. 28 (2018) 249–253.
[26] A. Mehta, M. Prabhakar, P. Kumar, et al., Excitotoxicity: Bridge to various triggers in neurodegenerative disorders, Eur. J. Pharmacol. 698 (2013) 6–18.
[27] R. Franco, J.A. Cidlowski, Glutathione efflux and cell death, Antioxid. Redox Signal 17 (2012) 1694–1713.
[28] Y.-T. Chan, N. Wang, Y. Feng, The toxicology and detoxification of Aconitum: Traditional and modern views, Chin. Med. 16 (2021), 61.
[29] X. Gao, J. Hu, X. Zhang, et al., Research progress of aconitine toxicity and forensic analysis of aconitine poisoning, Forensic. Sci. Res. 5 (2020) 25–31.
[30] J. Zhou, C. Peng, Q. Li, et al., Dopamine homeostasis imbalance and dopamine receptors-mediated AC/cAMP/PKA pathway activation are involved in aconitine-induced neurological impairment in zebrafish and SH-SY5Y cells, Front. Pharmacol. 13 (2022), 837810.
[31] X. Chen, R. Wu, H. Jin, et al., Successful rescue of a patient with acute aconitine poisoning complicated by polycystic renal hemorrhage, J. Nippon Med. Sch. 82 (2015) 257–261.
[32] Y. Gao, H. Fan, A. Nie, et al., Aconitine: A review of its pharmacokinetics, pharmacology, toxicology and detoxification, J. Ethnopharmacol. 293 (2022), 115270.
[33] X.X. Zheng, Y. Li, K.L. Yang, et al., Icariin reduces Glu-induced excitatory neurotoxicity via antioxidative and antiapoptotic pathways in SH-SY5Y cells, Phytother. Res. 35 (2021) 3377–3389.
[34] Z. Yang, J. Wang, C. Yu, et al., Inhibition of p38 MAPK signaling regulates the expression of EAAT2 in the brains of epileptic rats, Front. Neurol. 9 (2018), 925.
[35] L. Zong, J. Xing, S. Liu, et al., Cell metabolomics reveals the neurotoxicity mechanism of cadmium in PC12 cells, Ecotoxicol. Environ. Saf. 147 (2018) 26–33.

[36] X. Geng, J. Shen, F. Li, et al., Phosphoenolpyruvate carboxykinase (PCK) in the brain gluconeogenic pathway contributes to oxidative and lactic injury after stroke, Mol. Neurobiol. 58 (2021) 2309–2321.
[37] J. Yip, X. Geng, J. Shen, et al., Cerebral gluconeogenesis and diseases, Front. Pharmacol. 7 (2017), 521.
[38] L. Lu, J. Huang, J. Mo, et al., Exosomal lncRNA TUG1 from cancer-associated fibroblasts promotes liver cancer cell migration, invasion, and glycolysis by regulating the miR-524-5p/SIX1 axis, Cell. Mol. Biol. Lett. 27 (2022), 17.
[39] Q. Chu, Y. Li, Z. Hua, et al., *Tetrastigma hemsleyanum* vine flavone ameliorates glutamic acid-induced neurotoxicity via MAPK pathways, Oxid. Med. Cell. Longev. 2020 (2020), 7509612.
[40] J. Karch, J.D. Molkentin, Regulated necrotic cell death: The passive aggressive side of Bax and Bak, Circ. Res. 116 (2015) 1800–1809.
[41] W. Zhang, Q. Zhang, J. Lin, Cell analysis on microfluidics combined with mass spectrometry, Anal. Sci. 37 (2021) 249–260.
[42] S. Mao, W. Li, Q. Zhang, et al., Cell analysis on chip-mass spectrometry, Trends Analyt. Chem. 107 (2018) 43–59.